Stopped-flow fluorescence kinetic study of protein sliding and intersegment transfer in the target DNA search process

Alexandre Esadze, **Junji Iwahara**[*]

Department of Biochemistry & Molecular Biology, Sealy Center for Structural Biology and Molecular Biophysics, University of Texas Medical Branch, Galveston, TX 77555-1068, USA

Abstract

Kinetic characterizations of protein translocation on DNA are nontrivial because the simultaneous presence of multiple different mechanisms makes it difficult to extract the information specific to a particular translocation mechanism. In this study, we have developed new approaches for the kinetic investigations of proteins' sliding and intersegment transfer (also known as 'direct transfer') in the target DNA search process. Based on the analytical expression of the mean search time for the discrete–state stochastic model, we derived analytical forms of the apparent rate constant k_{app} for protein-target association in systems involving competitor DNA and the intersegment transfer mechanism. Our analytical forms of k_{app} facilitate the experimental determination of the kinetic rate constants for intersegment transfer and sliding in the target association process. Using stopped-flow fluorescence data for the target association kinetics along with the analytical forms of k_{app}, we have studied the translocation of the Egr-1 zinc-finger protein in the target DNA association process. Sliding was analyzed using the DNA length-dependent k_{app} data. Using the dependence of k_{app} on the concentration of competitor DNA, we determined the second-order rate constant for intersegment transfer. Our results indicate that a major pathway in the target association process for the Egr-1 zinc-finger protein is the one involving intersegment transfer to a nonspecific site and the subsequent sliding to the target.

Keywords

Protein-DNA interaction; Kinetics; Target search process; Stopped-flow; Fluorescence

Introduction

Since Riggs et al. discovered amazingly rapid target location by the *E. coli lac* repressor in 1970,[1] the mechanisms that allow DNA-binding proteins to efficiently locate their target DNA sites have been studied both experimentally and theoretically (e.g. reviews in refs [2–9]). It was shown that nonspecific DNA binding plays an important role in increasing the efficiency with which proteins locate their specific target DNA sites. Berg et al. conceptually defined three major mechanisms for protein translocation on DNA:[10] 1) sliding, 2)

[*]To whom correspondence should be addressed. Contact Information: [Address] 301 University Blvd, Medical Research Building 5.104B, Galveston, Texas 77555-1068, USA [Phone] 409-747-1403 [Fax] 409-772-6334, j.iwahara@utmb.edu.

dissociation and re-association, and 3) intersegment transfer (also known as direct transfer). Sliding is the random walk of protein while being bound to DNA and can be regarded as one-dimensional diffusion. Translocations via dissociation and re-association are categorized into long-range translocation to an uncorrelated site and short-range translocation (known as 'hopping') to a nearby site. Intersegment transfer is direct transfer of protein from one DNA duplex to another (without going through the intermediary of free protein) via an intermediate where a protein molecule transiently bridges two DNA duplexes.

These distinct translocation mechanisms can coexist, and their relative contributions to the overall efficiency of a target DNA search should depend on proteins. For example, intersegment transfer is considered to be unlikely for proteins that cannot bridge two DNA duplexes transiently. The efficiency of each translocation mechanism should also depend on environmental factors, such as ionic strength, DNA density, DNA geometry, and the presence of other proteins. Characterizing a particular translocation mechanism is difficult due to the simultaneous presence of distinct mechanisms, particularly when molecular ensembles are measured in bulk solutions. Recently, remarkable advancements in single-molecule biophysics enabled the direct observation of protein sliding on DNA.[3,11–17] Elegant biochemical methods were also developed for kinetic investigations of one-dimensional search.[18–25] These methodological advances have substantially deepened the understanding of protein sliding on DNA. However, there is a lack of experiment-based knowledge about the kinetics of the other translocation mechanisms and the interplay between the distinct mechanisms during the target search process.

The least understood of the above-mentioned major translocation mechanisms is intersegment transfer. While many theoretical papers on the target DNA search have overlooked intersegment transfer, recent experimental studies clearly showed the significance of intersegment transfer, at least for several proteins.[26–34] As explained below, intersegment transfer appears to be a second-order process and was studied via biochemical or biophysical measurements of apparent exchange[29,33,34] or dissociation[27,30,32] rates as a function of DNA concentration. Although previous studies suggested the importance of intersegment transfer, its actual kinetic contribution to the target association process remains to be addressed.

In this paper, we present a new theoretical framework and experimental approaches to quantitatively investigate the kinetics of intersegment transfer and sliding in the target association process. Using this methodology, we study the target search kinetics of the inducible transcription factor Egr-1 (also known as Zif268), which plays important roles in the brain and the cardiovascular system. In the brain, Egr-1 is induced by synaptic signals and activates genes for long-term memory formation and consolidation.[35,36] In the cardiovascular system, Egr-1 serves as a stress-inducible transcription factor that activates the genes for defense responses against vascular stress and injury.[37,38] Egr-1 recognizes a 9-bp target DNA sequence, GCGTGGGCG, via three zinc-finger domains.[39] Within its short lifetime (~½ – 1 hour),[37] the induced Egr-1 protein regulates a particular set of genes, allowing the cells to rapidly respond to the stimuli. It is thus important to understand how Egr-1 efficiently scans DNA. Our current study provides insights into the roles of sliding and intersegment transfer in the target search by Egr-1.

Theory

Here we provide the theoretical framework for our stopped-flow kinetic method that is applicable to proteins that form a stable complex with their target DNA site. The studied systems involve three macromolecular components: the probe DNA, protein, and nonspecific competitor DNA (Figure 1A). The probe DNA contains a target site and a fluorescent group that is tethered to a position near the target. The fluorescence from the probe changes upon binding of the protein to the target site. The time course of the change is monitored immediately after a solution of the protein is rapidly mixed with a solution containing the probe DNA and the competitor DNA. We specifically deal with systems in which the total concentrations of the protein, the probe DNA, and the competitor DNA (P_{tot}, D_{tot}, and C_{tot}, respectively) satisfy the following:

$$D_{tot} \ll P_{tot} \ll C_{tot}.$$ [1]

These conditions can be used only for proteins that exhibit high specificity to their target. Because of these inequalities, the relevant second-order processes occur in a pseudo-first-order manner, which simplifies the kinetic analysis of experimental data.[40] The fluorescence time-course data are used to determine an apparent pseudo-first-order rate constant, k_{app}, for binding of the target to the protein. Due to the large excess of competitor DNA, only one protein can bind to the probe DNA, which allows for accurate kinetic measurement of sliding without interference due to the presence of multiple protein molecules on the same DNA. Moreover, the target DNA search in the presence of a large excess of competitor DNA represents a more realistic case and provides insights into the search processes *in vivo*.

Intersegment transfer as a phenomenological second-order process

Intersegment transfer of a protein between two DNA duplexes can be represented by:

$$D_b + PD_a \underset{k_{d1}}{\overset{k_{f1}}{\rightleftarrows}} D_b PD_a \underset{k_{f2}}{\overset{k_{d2}}{\rightleftarrows}} PD_b + D_a$$ [2]
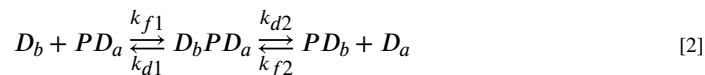
where PD represents a protein-DNA complex; $D_b PD_a$, the DNA-bridging intermediate; k_{f1} and k_{f2}, second-order rate constants for formation of the intermediate; and k_{d1} and k_{d2}, first-order rate constants for dissociation of the intermediate into a protein-DNA complex and free DNA. If the intermediate is a transient and low-population state, the intersegment transfer appears to be a second-order process:

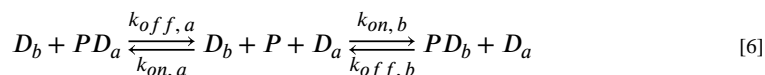$$D_b + PD_a \underset{k_{IT,ba}}{\overset{k_{IT,ab}}{\rightleftarrows}} PD_b + D_a.$$ [3]
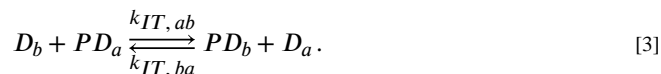
Using a steady-state approximation (Supplemental Information), the apparent second-order rate constants $k_{IT,ab}$ and $k_{IT,ba}$ are given by:

$$k_{IT,ab} = k_{f1}k_{d2}(k_{d1} + k_{d2})^{-1}$$ [4]

$$k_{IT,ba} = k_{f2}k_{d1}(k_{d1} + k_{d2})^{-1}.$$ [5]

If $k_{d1} = k_{d2}$ and the duplexes D_a and D_b exhibit the same affinity, then $k_{IT,ab} = k_{IT,ba} = \frac{1}{2}k_{f1} = \frac{1}{2}k_{f2}$. Because of the second-order nature, the overall rate for intersegment transfer is proportional to the free DNA concentration. In fact, this nature has been essential in the experimental detection of intersegment transfer.[27–30,32–34,41,42]

In contrast, the overall rate for translocation via dissociation and re-association is virtually independent of the free DNA concentration when the DNA concentration is higher than the dissociation constant K_d. This translocation is represented by:

$$D_b + PD_a \underset{k_{on,a}}{\overset{k_{off,a}}{\rightleftharpoons}} D_b + P + D_a \underset{k_{off,b}}{\overset{k_{on,b}}{\rightleftharpoons}} PD_b + D_a$$ [6]

When $[D] \gg K_d$, the rate limiting step for this scheme is the dissociation (a first-order process) because this inequality corresponds to $k_{off} \ll k_{on}[D]$. In this case, an increase in $[D]$ does not affect the overall rate because the rate-limiting step is of first order. Thus, intersegment transfer can be distinguished experimentally from translocation via dissociation and re-association.

Discrete-state kinetic model for target DNA search

Our kinetic model for a target DNA search assumes discrete states in nonspecific protein-DNA association and is similar to the model used by Veksler and Kolomeisky.[43] The discrete nature of nonspecific protein-DNA association is supported by the recent solution NMR studies on nonspecific protein-DNA complexes.[29,34,44–46] As shown in Figure 1B, the probe DNA in our model contains a total of L sites, of which only the m-th site from an edge is a target, and all the others are nonspecific sites. Competitor DNA contains a total of M nonspecific sites. Our kinetic model addresses dissociation, association, sliding, and intersegment transfer (Figure 1C). Based on the above-mentioned considerations, our kinetic model treats intersegment transfer as a second-order process between a protein-DNA complex and free DNA. Although intersegment transfer can occur between two distant sites on the same molecule if the DNA length is significantly longer than the persistence length (i.e., ~150 bp), such intra-molecular intersegment transfer is not considered here because only relatively short (< 150 bp) DNA duplexes are used in our experiments. The model involves the intrinsic (as opposed to apparent) association rate constants $k_{on,N}$ and $k_{on,S}$, the dissociation rate constants $k_{off,N}$ and $k_{off,S}$, the first-order rate constants $k_{sl,N}$ and $k_{sl,S}$ for sliding, and the second-order rate constants $k_{IT,N}$ and $k_{IT,S}$ for intersegment transfer (annotations N and S are for nonspecific and specific sites, respectively). These kinetic rate constants are schematically summarized in Figure 1C. A complete set of the rate equations for our kinetic model is given in the Supplemental Information. Numerical integration of the rate equations, which can readily be performed with a standard ordinary-differential-equation (ODE) solver, provides the populations of the individual species as a function of time (details given in the Supplemental Information). The ODE-based simulations allowed us to assess the analytical forms of k_{app} presented below.

Mean search time of the Veksler-Kolomeisky model

For systems involving neither competitor DNA nor intersegment transfer, Veksler and Kolomeisky derived a general analytical expression for the mean time T_P for a protein, which is initially in the free state, to reach the target:[43]

$$T_P = \{Lk_{out} + (L - S)k_{in}\}/(k_{out}k_{in}S).$$ [7]

In this expression, the relevant parameters are as follows:

$$k_{in} = Lk_{on,N}D_{tot}$$ [8]

$$k_{out} = k_{off,N}$$ [9]

$$S = y(1 + y)(y^{-L} - y^L)/\{(1 - y)(y^{1-m} + y^m)(y^{1+L-m} + y^{m-L})\}$$ [10]

$$y = 1 + (1/2)(k_{out}/k_{sl,N}) - \{(k_{out}/k_{sl,N}) + (1/4)(k_{out}/k_{sl,N})^2\}^{1/2},$$ [11]

where k_{in} is the rate constant for the free protein to bind to any site on the probe DNA; k_{out}, the rate constant for the bound protein to leave the probe DNA; L, the total number of sites; and m, the target position. Hereafter, this general analytical expression is referred to as the VK model.

k_{app} for systems involving competitor DNA in the absence of intersegment transfer

Now we address the systems involving competitor DNA under the conditions of $D_{tot} \ll P_{tot} \ll C_{tot}$. Owing to these inequalities, the association of proteins with the competitor DNA reaches quasi-equilibrium far more rapidly than the association with the target. Based on this assumption and the VK model, the apparent pseudo-first-order rate constant k_{app} for the target to bind to the protein in the absence of intersegment transfer is given by:

$$k_{app} = \frac{1}{T_P}\frac{f_P P_{tot}}{D_{tot}}\left\{1 + \frac{K_{d,S}}{f_P P_{tot}}\right\},$$ [12]

where f_p is the fraction of the protein in the free state:

$$f_P = K_{d,N}(K_{d,N} + \phi M C_{tot})^{-1}.$$ [13]

The derivation of Eq. 12 is provided in the Supplemental Information. $K_{d,N}(= k_{off,N}/k_{on,N})$ is the dissociation constant for *each* nonspecific site, and $K_{d,S}$ is the dissociation constant for the target. The parameter ϕ is the number of possible orientations for each nonspecific site. Due to structural pseudo-C2 symmetry for DNA, $\phi = 2$ for proteins that bind as monomer; $\phi = 1$ for symmetric dimers. When $\phi = 2$ is used, microscopic parameters (e.g., $K_{d,N}$, $k_{off,N}$, $k_{IT,N}$) are defined for each orientation. Additional considerations on systems with $\phi = 2$ are

given in the Supplemental Information. The k_{app} constants from this analytical expression (Eq. 12) agree well with those from the ODE-based simulations (Figure 2A).

VK model vs. Berg's approximation

For systems without competitor DNA, Berg et al. showed that if the target site is located in the middle of rod-like DNA, the apparent rate constant k_{app} can be approximated by:[10]

$$k_{app} = 2k_{on,N}P_{tot}\sqrt{\frac{D_1}{l^2 k_{off,N}}}\tanh\left(\frac{L}{2}\sqrt{\frac{l^2 k_{off,N}}{D_1}}\right)$$

[14]

where D_1 is a one-dimensional diffusion constant for sliding, and l is the distance between two adjacent sites (3.4 Å) along the DNA axis. This expression assumes an approximate continuum state for sliding, whereas the VK model assumes discrete states. It is straightforward to derive a simple relationship between D_1 and $k_{sl,N}$:

$$D_1 = l^2 k_{sl,N}.$$

[15]

Eq. 15 indicates that D_1 is equivalent to $k_{sl,N}$ when D_1 is given in bp^2 s^{-1}. For systems involving competitor DNA, Eq. 14 can be modified to the following:

$$k_{app} = 2k_{on,N}f_P P_{tot}\left\{1 + \frac{K_{d,S}}{f_P P_{tot}}\right\}\sqrt{\frac{k_{sl,N}}{k_{off,N}}}\tanh\left(\frac{L}{2}\sqrt{\frac{k_{off,N}}{k_{sl,N}}}\right).$$

[16]

As demonstrated in Figure 2B, the modified Berg's approximation (Eq. 16) provides an accurate k_{app} only if the target is located at $m \approx L/2$. This limitation occurs because Eqs. 14 and 16 assume that the antenna effect (i.e., enhancement of target association via association with nonspecific sites followed by sliding)[7,47] applies to the same degree for both sides of the target. When the target is located near the edge of the DNA, only one side provides a significant degree of the antenna effect, and therefore the search kinetics can slow down by up to ~2-fold.[43] The VK-model-based expression (Eq. 12) provides an accurate k_{app} for any m value, because this model accounts for different antenna effects for the two sides. This property of the VK-model-based expression is especially important when an extrinsic fluorescent group in close proximity to the target is used to detect the formation of the specific complex.

k_{app} for systems with competitor DNA in the presence of intersegment transfer

Under the condition of $D_{tot} \ll P_{tot} \ll C_{tot}$, the fraction of the protein bound to the competitor DNA (f_{CP}) is given by:

$$f_{CP} = \phi M C_{tot}(K_{d,N} + \phi M C_{tot})^{-1}$$

[17]

If intersegment transfer is efficient, a major pathway in the target association kinetics can be the pathway from the competitor DNA to the target via intersegment transfer and subsequent

sliding. Using the mean time T_{CP} for the search via this additional pathway, the k_{app} constant is given approximately by:

$$k_{app} = \left(\frac{f_P}{T_P} + \frac{f_{CP}}{T_{CP}}\right)\frac{P_{tot}}{D_{tot}}\left\{1 + \frac{K_{d,S}}{f_p P_{tot}}\right\}$$

[18]

Because the VK model does not assume any particular mechanisms for protein's arrival to and departure from the probe DNA, T_{CP} is given in the same form as T_P (i.e., Eqs 7–11), but with k_{in} and k_{out} substituted to:

$$k_{in,CP} = L k_{IT,N} D_{tot}$$

[19]

$$k_{out,CP} = k_{off,N} + \phi M k_{IT,N} C_{tot}.$$

[20]

The rate constant k_{out} for T_P should also be substituted to $k_{out,CP}$ for the systems involving the intersegment transfer mechanism because the protein on a nonspecific site of the probe DNA can leave the probe DNA via intersegment transfer as well (with a pseudo-first-order rate constant $\phi M k_{IT,N} C_{tot}$). As shown in Figure 3, the k_{app} constants calculated using this analytical expression (Eq. 18) agree well with those from the ODE-based numerical simulations.

Sliding and dependence of k_{app} on length of the probe DNA

Although some previous studies used the DNA-length dependence of target association to investigate sliding,[20,24,48–50] the previous analytical expressions (e.g. Eq. 14) were applicable only to systems involving neither competitor DNA nor intersegment transfer. With our analytical form of k_{app}, we can determine the rate constant $k_{sl,N}$ for sliding from experimental data for systems involving competitor DNA and intersegment transfer. In Eq. 18, the dependence of k_{app} on $k_{sl,N}$ arises from T_P and T_{CP}. Note that T_P and T_{CP} share exactly the same S (Eq. 10) and y (Eq. 11), which are the only parameters containing the rate constant $k_{sl,N}$ for sliding. Because of this similarity, the length dependence for Eq. 12 with k_{out} substituted to $k_{out,CP}$ is virtually indistinguishable from that for Eq. 18. The rate constants $k_{sl,N}$ can be accurately determined from length-dependent k_{app} data via nonlinear least-squares fitting with Eq. 12, even for systems involving intersegment transfer. This is convenient for experimental research. An important parameter for sliding is the effective sliding length λ given by:[43]

$$\lambda = \left(k_{sl,N}/k_{out}\right)^{1/2}.$$

[21]

Again, k_{out} should be substituted to $k_{out,CP}$ if intersegment transfer is involved. As is evident from Eq. 11 (also from Eq. 16), λ is directly relevant to the length dependence of k_{app}. When $L < \lambda$, k_{app} is virtually proportional to L because of the extended antenna effect. As noted previously, an increase in L beyond 2λ does not enhance the antenna effect.[7] Because this asymptotic length dependence is important for determining $k_{sl,N}$ and λ, the length L should be varied with the maximum being larger than (or at least comparable to) λ.

Intersegment transfer and dependence of k_{app} on concentration of competitor DNA

In the absence of intersegment transfer, the k_{app} constant is virtually proportional to C_{tot}^{-1} when $\phi M C_{tot} \gg K_{d,N}$ as noted by Lin and Riggs.[51] This proportionality is obvious from Eqs 12 and 13. At a higher concentration of competitor DNA, the protein can be trapped at nonspecific sites more easily, which slows down the target association process. However, intersegment transfer can counteract this trapping effect. In the presence of intersegment transfer, the escape of a protein from competitor DNA can become faster at a higher concentration of competitor DNA because intersegment transfer is a second-order process whose rate is proportional to the concentration of the DNA in the free state. When the f_{CP}/T_{CP} term in Eq. 18 is significantly larger than the f_P/T_P term, the dependence of k_{app} on C_{tot} becomes substantially weaker than the proportionality to C_{tot}^{-1}. By measuring k_{app} as a function of C_{tot}, the rate constant $k_{IT,N}$ for intersegment transfer can be determined via nonlinear least-squares fitting with Eq. 18. The term involving f_{CP}/T_{CP} in Eq. 18 corresponds to the contribution of the pathway that involves intersegment transfer followed by sliding to the overall target association kinetics. Thus, the role of intersegment transfer in the target association process can be directly assessed.

Results

In the current study, we investigated the target search kinetics for the DNA-binding domain of human Egr-1. Hereafter, this protein construct comprising three zinc fingers is referred to as the 'Egr-1 zinc-finger protein' for simplicity's sake. The association of the Egr-1 zinc-finger protein with DNA was monitored via the fluorescence from the fluorescent group that was covalently attached to a DNA terminus. We used the DNA duplexes shown in Figure 4.

Dissociation constants for nonspecific and specific complexes

Analyses of sliding and intersegment transfer based on the discrete kinetic model require the equilibrium constants for the nonspecific and specific complexes. We measured the affinities using 12-bp nonspecific and specific DNA duplexes with tetramethylrhodamine (TAMRA) attached to the 3'-terminus (Figure 4). The apparent K_d constants were determined from the fluorescence anisotropy as a function of protein concentration. TAMRA was used for the K_d measurements because it exhibits a large change in fluorescence anisotropy upon binding of the protein to DNA. We measured the apparent K_d for the 12-bp nonspecific DNA to be 0.58 ± 0.08 μM at 80 mM KCl (Figure 5). Because the previous structural studies for the specific and nonspecific DNA complexes of Egr-1 showed that Egr-1 binds to DNA as a monomer and covers 9 bp,[34,39] the 12-bp nonspecific DNA has 8 [$= 2 \times (12 - 9 + 1)$] overlapping sites (this number corresponds to ϕM). Assuming that the apparent K_d can be approximated by $k_{off,N}/(\phi M k_{on,N})$ in this case where only one protein molecule can bind to the 12-bp DNA, the dissociation constant $K_{d,N}$ for *each* nonspecific site was calculated to be 4.6 μM ($= 0.58 \times 8$). This value was used in the calculations to determine $k_{sl,N}$ and $k_{IT,N}$ (see below). For the 12-bp specific DNA containing the target site, the affinity at 80 mM KCl was too strong to directly measure with the same fluorescence method. However, we were able to measure the dissociation constant K_d at higher ionic strengths (Figure 5). By extrapolating from these data along with the counterion condensation theory,[52,53] $K_{d,S}$ at 80 mM KCl were estimated to be ~0.1 nM.

Change of FAM fluorescence intensity upon Egr-1 target association

To detect the binding of Egr-1 to the target site on the probe DNA duplexes, we monitored the change in fluorescence intensity of 5'-terminal fluorescein amidite (FAM), which was located near the Egr-1 target (at the second position from the terminus; see Figure 4). We chose this fluorescent probe for our stopped-flow kinetic experiments because the FAM-labeled DNA exhibited stronger fluorescence intensity (but weaker anisotropy) than the TAMRA-labeled DNA exhibited. The FAM emission spectra recorded for the 113-bp probe DNA in the presence and absence of the Egr-1 zinc-finger protein and competitor DNA are shown in Figure 6A. Although no spectral change was observed upon the addition of competitor DNA to the solution of probe DNA, a significant (up to ~18%) reduction in the fluorescence intensity was observed when the Egr-1 zinc-finger protein was added. This change in FAM fluorescence is presumably due to its close proximity to the DNA-bound protein, as observed for other proteins.[54,55] Varying the concentration of the Egr-1 zinc-finger protein, we measured the FAM fluorescence intensity from the probe DNA (2.5 nM) in the presence of 2 μM competitor DNA at equilibrium (Figure 6B). The titration data clearly show a high-affinity protein-DNA interaction with $K_d \ll 1$ nM at 80 mM KCl. This high affinity is consistent with the above-mentioned data for the 12-bp DNA containing a target site. Thus, these results indicate that the change in the FAM fluorescence intensity reflects the association of Egr-1 with the target (rather than other sites) on the probe DNA.

Target association kinetics for the Egr-1 zinc-finger protein

Using a stopped-flow device, we recorded the time courses of FAM fluorescence intensity immediately after mixing the protein solution with a solution containing the probe and competitor DNA duplexes. In this experiment, the emission light that passed through a long-pass filter (515 nm cutoff) was detected without using monochromator. Although this configuration allowed higher sensitivity, the percentage change in the emission intensity upon the target association was smaller due to a higher non-fluorescent background. Figure 6C shows the fluorescence time-course data obtained under conditions of $D_{tot} = 2.5$ nM, $P_{tot} = 50$ nM, and $C_{tot} = 2$ μM. Under these conditions together with the above-mentioned equilibrium constants, 95% of the protein molecules are bound to the 28-bp competitor DNA at the quasi-equilibrium that occurs immediately after mixing, and 96% of the target on the 113-bp DNA is bound to the protein at the conclusion of the binding reaction. To analyze the kinetics of distinct translocation mechanisms, we measured the apparent rate constant k_{app} using various settings of L, P_{tot}, and C_{tot} (all satisfying $D_{tot} \ll P_{tot} \ll C_{tot}$). In all cases, the fluorescence intensity changed in a mono-exponential manner, and an apparent pseudo-first-order rate constant k_{app} was determined via mono-exponential fitting. Figure 6D shows the dependence of k_{app} on P_{tot} in the presence of competitor DNA ($C_{tot} = 2$ μM). As our analytical forms (i.e., Eqs. 12, 16, and 18) predict, the rate constant k_{app} was proportional to P_{tot}. The slope of the plot corresponds to an apparent second-order rate constant k_a for target association ($k_a = 4.5 \times 10^7$ M^{-1} s^{-1} for Figure 6D). Although k_a was used in some previous studies of protein translocation on DNA,[20,25,48] we used the pseudo-first-order rate constant k_{app} instead when investigating sliding and intersegment transfer, as demonstrated below. This makes the investigations quicker yet remains equivalent to the use of k_a because k_{app} was found to be proportional to P_{tot} for all other conditions tested (Supplemental Information). In all the following experiments, we used $P_{tot} = 50$ nM, because at this

concentration, k_{app} was typically less than 5 s^{-1} and could be measured precisely (with errors < 10%) with our current method.

Dependence on the length of the probe DNA

To investigate the sliding kinetics of Egr-1 using dependence of k_{app} on the length of the probe DNA, we prepared 33-, 48-, 63-, 83-, 113- and 143-bp DNA duplexes, each containing a single target site and a FAM probe, as shown in Figure 4. With the stopped-flow fluorescence method, the rate constant k_{app} for target association was measured with 50 nM protein, 2.5 nM probe DNA, and 2,000 nM nonspecific DNA duplex (28 bp) at 80 mM KCl (Figure 7). As predicted in Figures 2 and 3, our experimental k_{app} data showed that the length dependence was an increasing function with a steeper slope for shorter lengths and an obvious asymptote for longer lengths. For example, the k_{app} constant for the 63-bp probe DNA was 64% larger than that for the 33-bp probe DNA, whereas the k_{app} constants for the 143-bp and 113-bp probe DNA duplexes were identical within experimental error. Qualitatively, these results suggest that the effective sliding length λ is comparable to the DNA lengths used in this experiment.

Kinetic rate constant for sliding of Egr-1 on DNA

The analytical forms of the k_{app} constants allow us to determine the sliding rate constant $k_{sl,N}$ from the length-dependent k_{app} data for Egr-1 in the system involving a large excess of competitor DNA. As described above, the determination of $k_{sl,N}$ does not require accurate information on intersegment transfer. For a DNA length > 30 bp, the effective diffusion coefficient ($D_{protein} + D_{DNA}$), which is relevant to the Smoluchowski limit, should be dominated by the three-dimensional diffusion coefficient $D_{protein}$ for the Egr-1 zinc-finger protein (10 kDa; hydrodynamic radius, ~15 Å). Therefore, the length dependence of the diffusion coefficient D_{DNA} for DNA does not have to be taken into consideration in the analysis of the length-dependent k_{app} data for the investigation of sliding.[10] Because Egr-1 binds to DNA as a monomer, Eq. 12 with $\phi = 2$ was employed for nonlinear least-squares fitting to determine the rate constant $k_{sl,N}$. The parameter L was set to $A - B + 1$, where A is the total length of DNA in bp and B is the length of each nonspecific site. As mentioned above, B was set to 9 bp. Thus, the values of L were 25, 40, 55, 80, 105, and 135 for the 33-bp, 48-bp, 63-bp, 88-bp, 113-bp and 143-bp probe DNA duplexes, respectively. The target position was $m = 2$ for all the probe DNA duplexes. Calculation of k_{app} using Eq. 12 requires four parameters: $k_{sl,N}$, k_{out}, $K_{d,N}$, and $K_{d,S}$. In the current case with $K_{d,S} / (f_{CP}P_{tot})$ << 1, information about $K_{d,S}$ is not essential in the calculation (see Eq. 12). With the experimentally obtained dissociation constant $K_{d,N}$, the rate constant $k_{on,N}$ was treated as $k_{off,N} / K_{d,N}$, while the other two parameters, $k_{sl,N}$ and k_{out}, were optimized via nonlinear least-squares fitting. The resultant best-fit curve is shown in Figure 7. The rate constant $k_{sl,N}$ was determined to be $(2.1 \pm 0.2) \times 10^5$ s^{-1} for the sliding of the Egr-1 zinc-finger protein at 80 mM KCl. This rate constant corresponds to $D_1 = (2.4 \pm 0.1) \times 10^{-2}$ μm^2 s^{-1}. Using Eq. 21, the effective sliding length λ was determined to be 50 ± 2 bp.

Dependence on the concentration of the competitor DNA

Using the 113-bp probe DNA, we measured the apparent rate constant k_{app} for target association at six different concentrations of competitor DNA ($C_{tot} = 0.5, 1.0, 2.0, 4.0, 6.0$

and 8.0 μM). The results are shown in Figure 8A. The k_{app} constant was found to decrease upon increasing C_{tot}. As described above, k_{app} should be virtually proportional to C_{tot}^{-1} if intersegment transfer is not involved in the target search process and $\phi M C_{tot} \gg K_{d,N}$. Although this inequality was satisfied, our data for the Egr-1 zinc-finger protein showed that k_{app} constant was not proportional to C_{tot}^{-1}. For example, our experiment showed that the ratio of the k_{app} constant at $C_{tot} = 2.0$ μM to that at $C_{tot} = 8.0$ μM was only 1.3, instead of 4. These results qualitatively suggest that intersegment transfer contributes significantly to the target association process.

Kinetic rate constant for intersegment transfer of Egr-1

Using the C_{tot}-dependent k_{app} data, we determined the rate constant $k_{IT,N}$ for intersegment transfer. The analytical form of k_{app} for systems involving intersegment transfer (Eq. 18) was employed for nonlinear least-squares fitting to determine $k_{IT,N}$. The calculation of k_{app} with Eq. 18 requires five parameters: $k_{IT,N}$, $k_{off,N}$, $k_{sl,N}$, $K_{d,N}$, and $K_{d,S}$. Again, in the current case with $K_{d,S} / (f_{CP}P_{tot}) \ll 1$, information about $K_{d,S}$ is not essential in the calculation. As described above, $k_{on,N}$ was treated as $k_{off,N} / K_{d,N}$. Because $k_{sl,N}$ was determined from the length-dependent k_{app} data, only two parameters, $k_{IT,N}$ and $k_{off,N}$, were optimized in the fitting calculation. This procedure provided an excellent fit to the experimental C_{tot}-dependence data (Figure 8A; solid curves). In contrast, fitting with Eq. 12 (no intersegment transfer) provided only a poor fit to the experimental C_{tot}-dependence data (Figure 8A; dotted curves). Because these two models for fitting differ in the degree of freedom, Akaike's information criterion (AIC) was used for model assessment. The AIC values for the fittings with Eqs 12 and 18 were 187.9 and 7.4, respectively. These results clearly indicate that the model that accounted for intersegment transfer is far better to describe the C_{tot}-dependent k_{app} data. The rate constant $k_{IT,N}$ for intersegment transfer was determined to be $(1.0 \pm 0.1) \times 10^6$ M^{-1} s^{-1} for the Egr-1 zinc-finger protein at 80 mM KCl. The kinetic parameters determined in our current study are summarized in Table I.

Intersegment transfer → sliding as the major pathway for target association

Our methodology permits kinetic measurements of intersegment transfer between nonspecific DNA sites in the presence of the target site. Owing to this unique feature, we can directly examine the role of intersegment transfer in the target association process. The analytical form of k_{app} (Eq. 18) for the system involving competitor DNA and intersegment transfer includes the contributions of two major pathways for target association (Figure 8B). The $T_P^{-1} f_P P_{tot} D_{tot}^{-1}$ term in Eq. 18 represents the contribution from the pathway involving the association of the free protein with a nonspecific site on the probe DNA and the subsequent sliding to the target ("Pathway 1"). The $T_{CP}^{-1} f_{CP} P_{tot} D_{tot}^{-1}$ term in Eq. 18 represents the contribution from the pathway involving the intersegment transfer of competitor-bound protein to a nonspecific site on the probe DNA and the subsequent sliding to the target ("Pathway 2"). From the obtained kinetic rate constants, the relative contribution of Pathway 2 in the presence of 2 μM competitor DNA was calculated to be 92%. This result clearly indicates the importance of intersegment transfer in the presence of a large excess of competitor DNA.

Discussion

Extremely efficient intersegment transfer of Egr-1 between nonspecific DNA sites

Our current study shows that intersegment transfer of Egr-1 between nonspecific DNA sites is extremely efficient. The intersegment transfer rate constant $k_{IT,N}$ is only two-fold smaller than the association rate constant $k_{on,N}$ (Table I). In our previous NMR study, the second-order rate constant for the intersegment transfer of Egr-1 between two different 28-bp nonspecific DNA duplexes was measured at 20 mM KCl to be 3.6×10^6 M^{-1} s^{-1}.[34] This value corresponds to $k_{IT,N} = 1.8 \times 10^5$ M^{-1} s^{-1}, assuming that the number of sites is $M = 20$ in 28-bp DNA (note that $k_{IT,N}$ is defined for each pair of departure and arrival sites). Although the value of $k_{IT,N} = 1.0 \times 10^6$ M^{-1} s^{-1} from our current study is ~6-fold larger, the difference in ionic strength (20 mM vs. 80 mM KCl) can easily account for this discrepancy. In fact, in the case of the HoxD9 homeodomain, the kinetic rate constant for intersegment transfer at 60 mM NaCl was 10-fold larger than that at 20 mM NaCl.[56] Interestingly, the intersegment transfer of Egr-1 between the target DNA sites is > million-fold slower ($k_{IT,S} = 0.8$ M^{-1} s^{-1}),[42] presumably due to the absence of domain motions that facilitate formation of the transient DNA-bridging intermediate for intersegment transfer.[34] Our current fluorescence data and the previous NMR data are consistent in that both indicate the very efficient intersegment transfer of Egr-1 between nonspecific DNA sites.

Intersegment transfer as a mechanism to counteract trapping by high-concentration DNA

Nonspecific binding to DNA can substantially enhance the protein-target association via the antenna effect and reduced dimensionality.[2–9] However, trapping by nonspecific sites can substantially slow down the target association process at a high concentration of DNA.[4,7] For example, Eq. 12 for the systems in the absence of intersegment transfer indicate that k_{app} constant is proportional to C_{tot}^{-1}, which represents a stronger trapping effect at a higher DNA concentration. However, our data (Figure 8) clearly show that this dependence on C_{tot} becomes significantly weaker in the presence of intersegment transfer, allowing the protein to find its target site efficiently.

Although intersegment transfer was defined as direct transfer between two DNA chains via a transient DNA-bridging intermediate (Scheme 2), this intermediate has never been directly observed experimentally, as far as we know. Only coarse-grained molecular dynamics (CGMD) simulations directly inferred the DNA-bridging intermediates in intersegment transfer.[34,57–59] If the breakage of the bridging intermediate is the rate-limiting step, intersegment transfer should appear to be a first-order process that cannot be detected by DNA concentration-dependence experiments. In such a case, the DNA-bridging intermediate should be a stable species. Intersegment transfer should appear to be a second-order process (Scheme 3) when the formation of the bridging intermediate via collision of a nonspecific complex and free DNA is the rate-limiting step. In this case, the DNA-bridging intermediate is a transient, low-population species. Intersegment transfer observed in the current and previous[26–34] studies are of this kind. Our previous studies using NMR spectroscopy and CGMD simulations suggested that local dissociation of one of the three zinc fingers could allow Egr-1 to transiently bridge two DNA duplexes during intersegment transfer.[34,60] However, as Sidorova et al. recently suggested,[32] the phenomenological second-order nature

of intersegment transfer can be explained without assuming the presence of DNA-bridging intermediates. Regardless of whether the DNA-bridging intermediates are actually involved or not, the second-order nature of intersegment transfer is important because it allows the protein to counteract trapping by nonspecific sites at a high concentration of DNA.

Relevance to the target association process *in vivo*

Because the DNA density is extremely high in the nucleus (~100 mg/ml),[61] the target search pathway involving intersegment transfer may also play a major role in the target association process *in vivo*, at least for Egr-1. The intersegment transfer between the two DNA ends of a nucleosome particle may occur efficiently because the two ends are separated by only ~60 Å in three-dimensional space.[62] In fact, the CGMD simulations showed that Egr-1 could undergo rapid intersegment transfer between two DNA duplexes separated by this distance. [34] Thus, extremely efficient intersegment transfer, which was observed *in vitro* in our current and previous studies, may allow Egr-1 to effectively bypass nucleosome particles and to rapidly locate the target sites *in vivo*.

Egr-1's sliding on DNA: Comparison with other proteins

The one-dimensional diffusion coefficient D_I for sliding on DNA is known for some proteins. For example, $D_I = 4.8 \times 10^6$ bp^2 s^{-1} (0.55 μm^2 s^{-1}) for OGG1;[12] $D_I = 2.6 \times 10^6$ bp^2 s^{-1} (0.30 μm^2 s^{-1}) for p53;[63] $D_I = 4.9 \times 10^5$ bp^2 s^{-1} (5.7×10^{-2} μm^2 s^{-1}) for MutSα;[14] $D_I = 9.5 \times 10^4$ bp^2 s^{-1} (1.1×10^{-2} μm^2 s^{-1}) for EcoRV;[64] and $D_I = 3.0 \times 10^4$ bp^2 s^{-1} (3.5×10^{-3} μm^2 s^{-1}) for EcoRI.[22] In most of these studies, sliding on DNA was directly observed with single-molecule fluorescence techniques. As noted previously,[5,63] the single-molecule techniques could overestimate D_I due to their limited spatial resolution, which makes it difficult to distinguish sliding and hopping. Thus, D_I measurements with completely different principles are of practical importance. Our current bulk-solution study shows that $D_I = 2.1 \times 10^5$ bp^2 s^{-1} (2.4×10^{-2} μm^2 s^{-1}) for the Egr-1 zinc-finger protein (Table I). This value is within the typical range for the D_I coefficients. Unlike three-dimensional diffusion coefficients in solvent, the one-dimensional diffusion coefficient D_I for proteins sliding on DNA appears to be virtually independent of the molecular size. The number of intermolecular hydrogen bonds and ion pairs between protein and DNA in nonspecific complexes could be more important determinants of D_I.

Conclusions

We have studied the kinetics of Egr-1's sliding and intersegment transfer in the target DNA search process. We have derived the analytical forms of k_{app} that facilitate kinetic investigations of distinct translocation mechanisms in the presence of a large excess of nonspecific competitor DNA. The stopped-flow fluorescence data along with the analytical forms of k_{app} permit the determination of the rate constants for sliding and intersegment transfer for proteins that form a stable complex with their target. The most important finding in this work is that intersegment transfer plays a major role in the target association process. Although this role has been speculated in previous studies on intersegment transfer in the absence of the target, those studies could not provide information on the extent to which intersegment transfer can actually contribute to the target association kinetics. Owing to the

analytical expressions for k_{app}, our current methodology provides the relative contributions of distinct translocation pathways to target association. For the Egr-1 zinc-finger protein, the major pathway involves the intersegment transfer to a nonspecific site and the subsequent sliding to the target on the probe DNA. The relative contribution of this pathway was 92% for the system with 2.5 nM 113-bp probe DNA and 2,000 nM 28-bp nonspecific competitor DNA at 80 mM KCl. The corresponding contribution of the pathway involving the free protein's association with a nonspecific site and the subsequent sliding to the target was as small as 8%. Despite its significant contribution, translocation via intersegment transfer cannot be distinguished from translocation via dissociation and association unless the DNA concentration dependence is studied. This nature is most likely responsible for a delay in the understanding of intersegment transfer in the current field. We hope that our present work will stimulate further investigations on the target search pathways involving intersegment transfer for other transcription factors as well as for DNA repair/modifying enzymes.

Materials and Methods

Egr-1 zinc-finger protein:

The DNA-binding domain of human Egr-1 comprising three zinc fingers (residues 335–432) was expressed in *E. coli* BL21(DE3) and purified as described in our previous papers.[34,42] The Egr-1 solution was treated with 3 mM TCEP at 4 ˚C overnight to completely reduce the protein, and the buffer was extensively exchanged to 10 mM Tris•HCl (pH 7.5), 300 mM KCl, 1 mM 2-mercaptoethanol, and 200 nM $ZnCl_2$. The protein was quantified using a BCA assay kit (Pierce) or using UV absorbance at 280 nm and an extinction coefficient of 1490 mM^{-1} cm^{-1} (the results from these two methods were consistent). The protein solution was kept under argon gas until use.

Fluorescence-labeled probe DNA for kinetics measurements:

To prepare the DNA duplexes shown in Figure 4A, 33-mer single-stranded DNA with a FAM attached to the 5'-terminus was purchased from Integrated DNA Technology (IDT). Of the 33 bases, the first 12 bases contain an Egr-1 target sequence (9 bp) and the last 21 bases can hybridize with positions 1160–1180 of the pUC-19 plasmid. The DNA duplexes of 63, 88, 113, and 143 bp were prepared via PCR using Vent DNA polymerase (New England), the FAM-labeled 33-mer primer, a reverse primer, and pUC-19 as the template. The 48-bp duplex was prepared via hybridizing the FAM-labeled 33-mer and a singled-stranded DNA, followed by base filling with DNA polymerase. The 33-bp duplex was prepared via annealing of equimolar amounts of individual complementary strands. The FAM-labeled 33-bp duplex was purified via polyacrylamide gel electrophoresis (PAGE) using 4–20% gradient polyacrylamide / TBE gels (Invitrogen). The other duplexes (i.e., 48-, 63-, 88-, 113- and 143-bp) were purified through the following three procedures. First, the reaction mixture was loaded onto a Resource-Q anion-exchange column (GE Healthcare), and the DNA was eluted with a gradient of 0 – 1.5 M NaCl in a buffer of 50 mM Tris•HCl (pH 7.5) and 1 mM EDTA. The fractions containing the desired reaction product were concentrated and subjected to PAGE with 4–20% gradient polyacrylamide / TBE gels. The band of the desired PCR product was excised, crushed, and shaken at room temperature in a buffer of 10 mM

Tris•HCl (pH 7.5) and 40 mM KCl for 24 – 36 hours to extract the DNA from the gel. The extracted DNA duplexes were further purified via a PCR purification kit (Qiagen).

Competitor DNA:

The 28-bp nonspecific competitor DNA used for the kinetic experiments was the same as that used for the NMR studies of the Egr-1 - nonspecific DNA complex. This DNA was synthesized and purified as described previously.[34]

Stopped-flow fluorescence-based assay of target association kinetics:

The kinetics of target association was measured at 20 ˚C with an ISS PC-1 spectrofluorometer equipped with an Applied Photophysics Rx-2000 stopped-flow device. The following two solutions were mixed: Solution A: 50–200 nM protein in a buffer of 10 mM Tris•HCl (pH 7.5), 80 mM KCl, and 200 nM $ZnCl_2$; and Solution B: 5 nM FAM-labeled DNA and 1000–8000 nM 28-bp competitor DNA in the same buffer. The mixing ratio was 1:1; thus, the final concentrations of the protein and DNA became halved. The spectrofluorometer has two emission channels in a T-format: one with and the other without an emission-light monochromator. In the stopped-flow kinetics experiments, we used the emission channel with no monochromator for better sensitivity. The FAM fluorophore was excited at 460 nm, and the emission light that passed through a long-pass filter with a cutoff at 515 nm (Edmund Optics) was recorded. Immediately after stopping the flow for mixing, the time-course data of the fluorescence intensity were collected for 4–10 s with a time interval of 20–50 ms. Each experiment was repeated 8 to 10 times. As expected from the ODE-based numerical simulations, the time-course data of the fluorescence intensity were found to be mono-exponential. The apparent pseudo-first-order rate constant k_{app} for target association was determined from the experimental data via nonlinear least-squares fitting with $f(t) = f_\infty + (f_0 - f_\infty)\exp(-k_{app}t)$, where f_0, f_∞, and k_{app} are optimized, and $f(t)$ represents the fluorescence intensity.

Fluorescence anisotropy-based affinity measurements:

The two 12-bp DNA duplexes with a 3'-terminal TAMRA were prepared for affinity measurements (Figure 4B). HPLC-purified DNA strands from 250-nmol scale syntheses were purchased from Integrated DNA Technology. The complementary strands were mixed and annealed at 85 ˚C, and the duplex was purified by PAGE using 4–20% gradient polyacrylamide / TBE gels. The protein-titration experiments were performed at various concentrations of KCl in a buffer of 10 mM Tris•HCl (pH 7.5). The fluorescence anisotropy of the TAMRA-labeled DNA was measured at an excitation wavelength of 533 nm and emission wavelength of 580 nm using an ISS PC-1 spectrofluorometer. Because the K_d for specific complexes at low ionic strength was lower than the detection limit of the fluorescence method, we measured the K_d at higher ionic strengths (150, 200, 250, 300, 350, and 400 mM KCl) and extrapolated to the K_d at 80 mM KCl under the assumption of a linear relationship between $\log[KCl]$ and $\log K_d$ based on the counterion condensation theory.[52,53]

Determination of the rate constants for protein translocation:

Using the Levenberg-Marquardt algorithm of MATLAB, the rate constant $k_{sl,N}$ for sliding was determined from the length-dependent k_{app} data (Figure 7) via nonlinear least-squares fitting with Eqs. 7–13. The total numbers of binding sites, L for the probe DNA and M for the competitor DNA, were calculated as $A - B + 1$, where A is the total number of base pairs, and B is the number of base pairs covered by a protein molecule. Based on structural information,[34,39] $B = 9$ was used. Based on the sequences of the probe DNA duplexes (Figure 4), $m = 2$ was used. The values of $k_{off,N}$, and $k_{it,N}$ were determined from the C_{tot}-dependent k_{app} data (Figure 8) via nonlinear least-squares fitting with Eqs 7, 10, 11, 13, and 17–20. These calculations used $\phi = 2$ and $k_{on,N} = k_{off,N} / K_{d,N}$. The MATLAB scripts for the ODE-based simulations of the target search kinetics and those for determination of the kinetic parameters via fitting to experimental data are available as the 'TDSK' (target DNA search kinetics) package upon request to the corresponding author.

Supplementary Material

Refer to Web version on PubMed Central for supplementary material.

Acknowledgments

References

1. Riggs AD, Bourgeois S & Cohn M (1970). The lac repressor-operator interaction. 3. Kinetic studies. J Mol Biol 53, 401–17. [PubMed: 4924006]

2. Bruinsma RF (2002). Physics of protein-DNA interaction. Physica a-Statistical Mechanics and Its Applications 313, 211–237.

3. Gorman J & Greene EC (2008). Visualizing one-dimensional diffusion of proteins along DNA. Nat Struct Mol Biol 15, 768–74. [PubMed: 18679428]

4. Halford SE (2009). An end to 40 years of mistakes in DNA-protein association kinetics? Biochem Soc Trans 37, 343–8. [PubMed: 19290859]

5. Halford SE & Marko JF (2004). How do site-specific DNA-binding proteins find their targets? Nucleic Acids Res 32, 3040–52. [PubMed: 15178741]

6. Kolomeisky AB (2011). Physics of protein-DNA interactions: mechanisms of facilitated target search. Phys Chem Chem Phys 13, 2088–95. [PubMed: 21113556]

7. Mirny L, Slutsky M, Wunderlich Z, Tafvizi A, Leith J & Kosmrlj A (2009). How a protein searches for its site on DNA: the mechanism of facilitated diffusion. J Phys A: Math Theor 42, 401335.

8. Tafvizi A, Mirny LA & van Oijen AM (2011). Dancing on DNA: kinetic aspects of search processes on DNA. Chemphyschem 12, 1481–9. [PubMed: 21560221]

9. von Hippel PH & Berg OG (1989). Facilitated target location in biological systems. J Biol Chem 264, 675–8. [PubMed: 2642903]

10. Berg OG, Winter RB & von Hippel PH (1981). Diffusion-driven mechanisms of protein translocation on nucleic acids. 1. Models and theory. Biochemistry 20, 6929–48. [PubMed: 7317363]

11. Blainey PC, Luo G, Kou SC, Mangel WF, Verdine GL, Bagchi B & Xie XS (2009). Nonspecifically bound proteins spin while diffusing along DNA. Nat Struct Mol Biol 16, 1224–9. [PubMed: 19898474]

12. Blainey PC, van Oijen AM, Banerjee A, Verdine GL & Xie XS (2006). A base-excision DNA-repair protein finds intrahelical lesion bases by fast sliding in contact with DNA. Proc Natl Acad Sci U S A 103, 5752–7. [PubMed: 16585517]

13. Finkelstein IJ, Visnapuu ML & Greene EC (2010). Single-molecule imaging reveals mechanisms of protein disruption by a DNA translocase. Nature 468, 983–7. [PubMed: 21107319]

14. Gorman J, Wang F, Redding S, Plys AJ, Fazio T, Wind S, Alani EE & Greene EC (2012). Single-molecule imaging reveals target-search mechanisms during DNA mismatch repair. Proc Natl Acad Sci U S A 109, E3074–83. [PubMed: 23012240]

15. Hammar P, Leroy P, Mahmutovic A, Marklund EG, Berg OG & Elf J (2012). The lac repressor displays facilitated diffusion in living cells. Science 336, 1595–8. [PubMed: 22723426]

16. Leith JS, Tafvizi A, Huang F, Uspal WE, Doyle PS, Fersht AR, Mirny LA & van Oijen AM (2012). Sequence-dependent sliding kinetics of p53. Proc Natl Acad Sci U S A 109, 16552–7. [PubMed: 23012405]

17. Tafvizi A, Huang F, Fersht AR, Mirny LA & van Oijen AM (2011). A single-molecule characterization of p53 search on DNA. Proc Natl Acad Sci U S A 108, 563–8. [PubMed: 21178072]

18. Gowers DM, Wilson GG & Halford SE (2005). Measurement of the contributions of 1D and 3D pathways to the translocation of a protein along DNA. Proc Natl Acad Sci U S A 102, 15883–8. [PubMed: 16243975]

19. Jack WE, Terry BJ & Modrich P (1982). Involvement of outside DNA sequences in the major kinetic path by which EcoRI endonuclease locates and leaves its recognition sequence. Proc Natl Acad Sci U S A 79, 4010–4. [PubMed: 6287460]

20. Kim JG, Takeda Y, Matthews BW & Anderson WF (1987). Kinetic studies on Cro repressor-operator DNA interaction. J Mol Biol 196, 149–58. [PubMed: 2958636]

21. Porecha RH & Stivers JT (2008). Uracil DNA glycosylase uses DNA hopping and short-range sliding to trap extrahelical uracils. Proc Natl Acad Sci U S A 105, 10791–6. [PubMed: 18669665]

22. Rau DC & Sidorova NY (2010). Diffusion of the restriction nuclease EcoRI along DNA. J Mol Biol 395, 408–16. [PubMed: 19874828]

23. Schonhoft JD & Stivers JT (2012). Timing facilitated site transfer of an enzyme on DNA. Nat Chem Biol 8, 205–10. [PubMed: 22231272]

24. Stanford NP, Szczelkun MD, Marko JF & Halford SE (2000). One- and three-dimensional pathways for proteins to reach specific DNA sites. EMBO J 19, 6546–57. [PubMed: 11101527]

25. Winter RB, Berg OG & von Hippel PH (1981). Diffusion-driven mechanisms of protein translocation on nucleic acids. 3. The Escherichia coli lac repressor--operator interaction: kinetic measurements and conclusions. Biochemistry 20, 6961–77. [PubMed: 7032584]

26. Doucleff M & Clore GM (2008). Global jumping and domain-specific intersegment transfer between DNA cognate sites of the multidomain transcription factor Oct-1. Proc Natl Acad Sci U S A 105, 13871–6. [PubMed: 18772384]

27. Fried MG & Crothers DM (1984). Kinetics and mechanism in the reaction of gene regulatory proteins with DNA. J Mol Biol 172, 263–82. [PubMed: 6319716]

28. Iwahara J & Clore GM (2006). Direct observation of enhanced translocation of a homeodomain between DNA cognate sites by NMR exchange spectroscopy. J Am Chem Soc 128, 404–5. [PubMed: 16402815]

29. Iwahara J, Zweckstetter M & Clore GM (2006). NMR structural and kinetic characterization of a homeodomain diffusing and hopping on nonspecific DNA. Proc Natl Acad Sci U S A 103, 15062–7. [PubMed: 17008406]

30. Lieberman BA & Nordeen SK (1997). DNA intersegment transfer, how steroid receptors search for a target site. J Biol Chem 272, 1061–8. [PubMed: 8995403]

31. Sahu D, Clore GM & Iwahara J (2007). TROSY-based z-Exchange Spectroscopy: Application to the determination of the activation energy for intermolecular protein translocation between specific sites on different DNA molecules. J Am Chem Soc 129, 13232–13237. [PubMed: 17918842]

32. Sidorova NY, Scott T & Rau DC (2013). DNA concentration-dependent dissociation of EcoRI: direct transfer or reaction during hopping. Biophys J 104, 1296–303. [PubMed: 23528089]

33. Takayama Y & Clore GM (2012). Interplay between minor and major groove-binding transcription factors Sox2 and Oct1 in translocation on DNA studied by paramagnetic and diamagnetic NMR. J Biol Chem 287, 14349–63. [PubMed: 22396547]

34. Zandarashvili L, Vuzman D, Esadze A, Takayama Y, Sahu D, Levy Y & Iwahara J (2012). Asymmetrical roles of zinc fingers in dynamic DNA-scanning process by the inducible transcription factor Egr-1. Proc Natl Acad Sci U S A 109, E1724–32. [PubMed: 22675124]

35. Bozon B, Davis S & Laroche S (2003). A requirement for the immediate early gene zif268 in reconsolidation of recognition memory after retrieval. Neuron 40, 695–701. [PubMed: 14622575]

36. Lee JL, Everitt BJ & Thomas KL (2004). Independent cellular processes for hippocampal memory consolidation and reconsolidation. Science 304, 839–43. [PubMed: 15073322]

37. Khachigian LM, Lindner V, Williams AJ & Collins T (1996). Egr-1-induced endothelial gene expression: a common theme in vascular injury. Science 271, 1427–31. [PubMed: 8596917]

38. Yan SF, Fujita T, Lu J, Okada K, Shan Zou Y, Mackman N, Pinsky DJ & Stern DM (2000). Egr-1, a master switch coordinating upregulation of divergent gene families underlying ischemic stress. Nat Med 6, 1355–61. [PubMed: 11100120]

39. Pavletich NP & Pabo CO (1991). Zinc finger-DNA recognition: crystal structure of a Zif268-DNA complex at 2.1 Å. Science 252, 809–17. [PubMed: 2028256]

40. Pollard TD & De La Cruz EM (2013). Take advantage of time in your experiments: a guide to simple, informative kinetics assays. Mol Biol Cell 24, 1103–10. [PubMed: 23580192]

41. Bresloff JL & Crothers DM (1975). DNA-ethidium reaction kinetics: demonstration of direct ligand transfer between DNA binding sites. J Mol Biol 95, 103–23. [PubMed: 1171251]

42. Takayama Y, Sahu D & Iwahara J (2010). NMR studies of translocation of the Zif268 protein between its target DNA Sites. Biochemistry 49, 7998–8005. [PubMed: 20718505]

43. Veksler A & Kolomeisky AB (2013). Speed-Selectivity Paradox in the Protein Search for Targets on DNA: Is It Real or Not? J Phys Chem B.

44. Iwahara J, Schwieters CD & Clore GM (2004). Characterization of nonspecific protein-DNA interactions by ^{1}H paramagnetic relaxation enhancement. J Am Chem Soc 126, 12800–8. [PubMed: 15469275]

45. Kalodimos CG, Biris N, Bonvin AM, Levandoski MM, Guennuegues M, Boelens R & Kaptein R (2004). Structure and flexibility adaptation in nonspecific and specific protein-DNA complexes. Science 305, 386–9. [PubMed: 15256668]

46. Takayama Y & Clore GM (2011). Intra- and intermolecular translocation of the bi-domain transcription factor Oct1 characterized by liquid crystal and paramagnetic NMR. Proc Natl Acad Sci U S A 108, E169–76. [PubMed: 21555551]

47. Hu T, Grosberg AY & Shklovskii BI (2006). How proteins search for their specific sites on DNA: the role of DNA conformation. Biophys J 90, 2731–44. [PubMed: 16461402]

48. Berg OG & Ehrenberg M (1982). Association kinetics with coupled three- and one-dimensional diffusion. Chain-length dependence of the association rate of specific DNA sites. Biophys Chem 15, 41–51. [PubMed: 7074207]

49. Terry BJ, Jack WE & Modrich P (1985). Facilitated diffusion during catalysis by EcoRI endonuclease. Nonspecific interactions in EcoRI catalysis. J Biol Chem 260, 13130–7. [PubMed: 2997157]

50. Zhou HX (2005). A model for the mediation of processivity of DNA-targeting proteins by nonspecific binding: dependence on DNA length and presence of obstacles. Biophys J 88, 1608–15. [PubMed: 15596498]

51. Lin SY & Riggs AD (1972). Lac repressor binding to non-operator DNA: detailed studies and a comparison of eequilibrium and rate competition methods. J Mol Biol 72, 671–90. [PubMed: 4573844]

52. Manning GS (1978). Molecular Theory of Polyelectrolyte Solutions with Applications to Electrostatic Properties of Polynucleotides. Q Rev Biophys 11, 179–246. [PubMed: 353876]

53. Record MT, Anderson CF & Lohman TM (1978). Thermodynamic Analysis of Ion Effects on Binding and Conformational Equilibria of Proteins and Nucleic-Acids - Roles of Ion Association

or Release, Screening, and Ion Effects on Water Activity. Q Rev Biophys 11, 103–178. [PubMed: 353875]

54. Anderson BJ, Larkin C, Guja K & Schildbach JF (2008). Using fluorophore-labeled oligonucleotides to measure affinities of protein-DNA interactions. Methods Enzymol 450, 253–72. [PubMed: 19152864]

55. Lakowicz JR (2006). Principles of fluorescence spectroscopy. 3 edit, Springer, New York.

56. Iwahara J & Clore GM (2006). Detecting transient intermediates in macromolecular binding by paramagnetic NMR. Nature 440, 1227–30. [PubMed: 16642002]

57. Vuzman D, Azia A & Levy Y (2010). Searching DNA via a "Monkey Bar" mechanism: the significance of disordered tails. J Mol Biol 396, 674–84. [PubMed: 19958775]

58. Vuzman D & Levy Y (2010). DNA search efficiency is modulated by charge composition and distribution in the intrinsically disordered tail. Proc Natl Acad Sci U S A 107, 21004–9. [PubMed: 21078959]

59. Vuzman D, Polonsky M & Levy Y (2010). Facilitated DNA search by multidomain transcription factors: cross talk via a flexible linker. Biophys J 99, 1202–11. [PubMed: 20713004]

60. Iwahara J & Levy Y (2013). Speed-stability paradox in DNA-scanning by zinc-finger proteins. Transcription 4, 58–61. [PubMed: 23412360]

61. Lewin B (2000). Genes VII, Oxford Univ Press, Oxford.

62. Luger K, Mader AW, Richmond RK, Sargent DF & Richmond TJ (1997). Crystal structure of the nucleosome core particle at 2.8 Å resolution. Nature 389, 251–60. [PubMed: 9305837]

63. Tafvizi A, Huang F, Leith JS, Fersht AR, Mirny LA & van Oijen AM (2008). Tumor suppressor p53 slides on DNA with low friction and high stability. Biophys 95, L01–3. [PubMed: 18424488]

64. Bonnet I, Biebricher A, Porte PL, Loverdo C, Benichou O, Voituriez R, Escude C, Wende W, Pingoud A & Desbiolles P (2008). Sliding and jumping of single EcoRV restriction enzymes on non-cognate DNA. Nucleic Acids Res 36, 4118–27. [PubMed: 18544605]
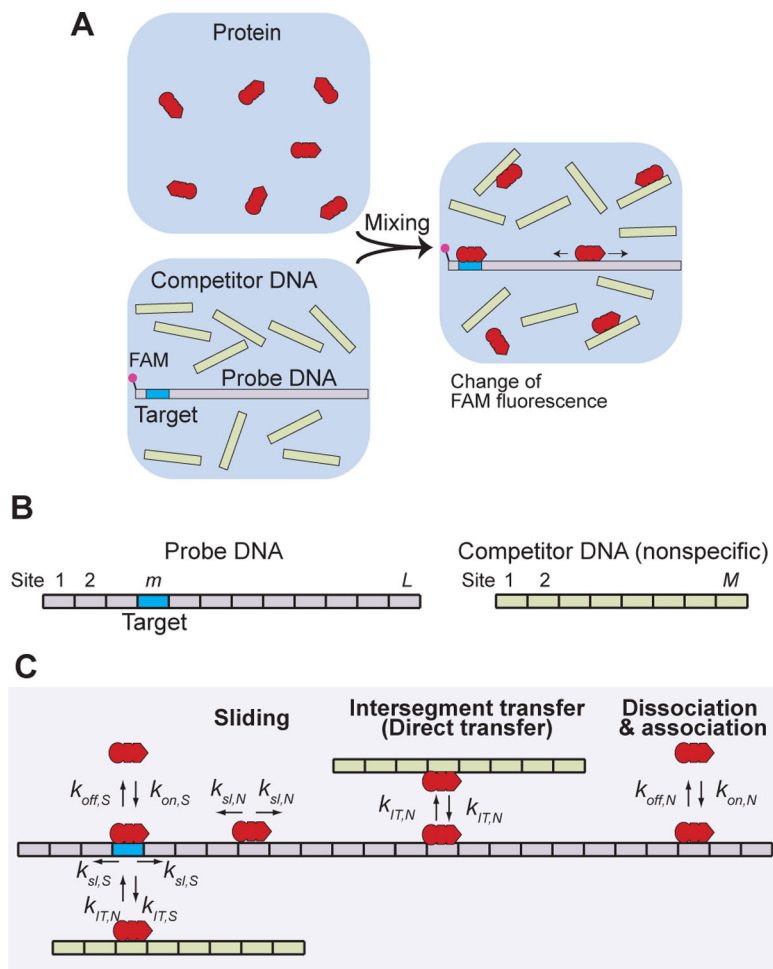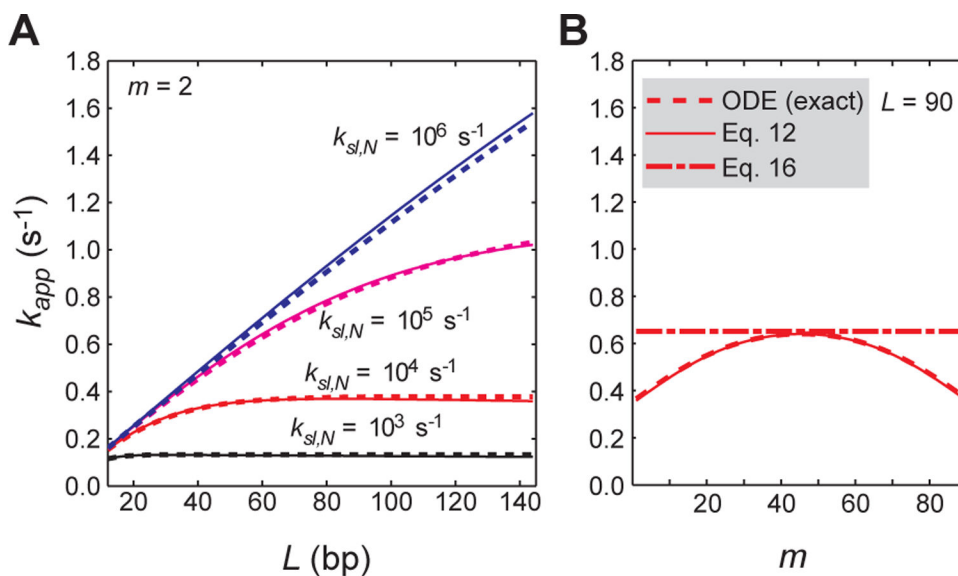
Figure 1.

Experimental design and kinetic model used in this study. (**A**) Stopped-flow fluorescence assay of the target DNA search kinetics. (**B**) Discrete binding sites on the probe and competitor DNA duplexes. (**C**) Rate constants involved in our kinetic model for the target association process. The rate constants $k_{sl,N}$ and $k_{sl,S}$ for sliding and the rate constants $k_{off,N}$ and $k_{off,S}$ for dissociation are first-order rate constants (units, s^{-1}), whereas the rate constants $k_{IT,N}$ and $k_{IT,S}$ for intersegment transfer and the rate constants $k_{on,N}$ and $k_{on,S}$ for association are second-order rate constants (units, M^{-1} s^{-1}). A rate constant for sliding is defined for sliding from one site to an adjacent site (i.e., shift by 1 bp). The rate constant $k_{sl,N}$ is related to the one-dimensional diffusion coefficient D_I for sliding, as indicated by Eq. 15. A complete set of rate equations for this kinetic model is given in the Supplemental Information.

Figure 2.
Validation of the VK model-based analytical form of k_{app} (Eq. 12) for systems involving competitor DNA but with no intersegment transfer. (**A**) Rate constant k_{app} for target association as a function of the total number of sites L. The position of the target was set to $m = 2$. The dashed lines were obtained from the ODE-based numerical kinetics simulations. The solid lines were obtained using Eq. 12. $k_{sl,N} = 10^3$, 10^4, 10^5, and 10^6 s^{-1} and $k_{off,N} = 10$ s^{-1} were used. Under these conditions, effective sliding lengths λ are 10 (black), 32 (red), 100 (magenta), and 316 (blue) bp. (**B**) Rate constants k_{app} as a function of the target position m for probe DNA with $L = 90$. For this panel, $k_{sl,N} = 10^4$ s^{-1} and $k_{off,N} = 10$ s^{-1} (an effective sliding length $\lambda = 32$ bp) were used. The dotted line is from the ODE-based numerical simulations; the solid line, from the VK model-based analytical form of k_{app} (Eq. 12); and the dashed line, from the modified Berg's approximation (Eq. 16). For both panels A and B, $D_{tot} = 2.5$ nM; $P_{tot} = 50$ nM, $K_{d,N} = 4$ μM; $K_{d,S} = 0.1$ nM; $C_{tot} = 2$ μM; $\phi = 1$; and $M = 20$.
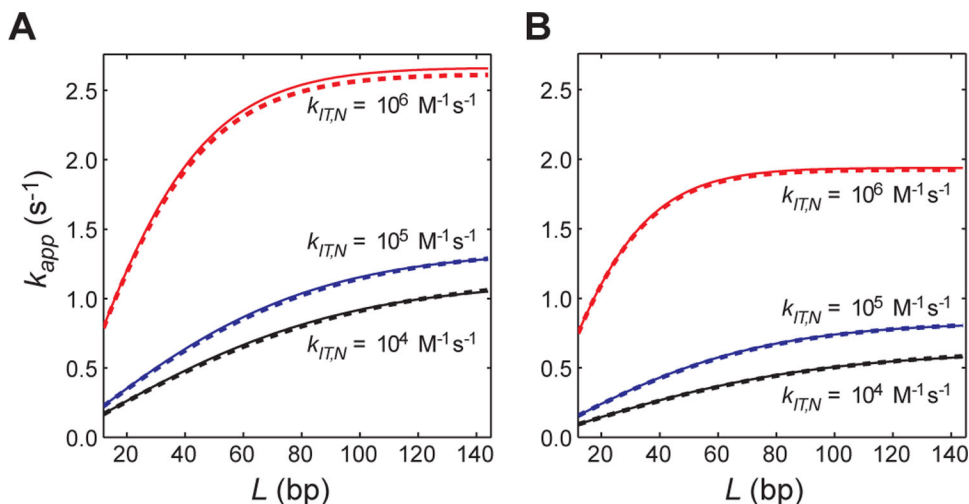
Figure 3.
Validation of the VK model-based analytical forms of k_{app} for systems involving competitor DNA and intersegment transfer (Eq. 18). (**A**) Rate constant k_{app} for target association as a function of the total number of sites L. A single orientation per site (i.e., $\phi = 1$) was assumed. The sliding rate constant $k_{sl,N} = 10^5$ s^{-1} was used. The other conditions are exactly the same as those for Figure 2A except that intersegment transfer is taken into consideration. The rate constants for intersegment transfer are indicated. (**B**) Rate constant k_{app} for target association as a function of the total number of sites L under conditions identical to those for the panel A, except that 2 orientations per site are assumed (i.e., $\phi = 2$). The kinetic and thermodynamic parameters are defined for each orientation. For both panels, the dashed lines were obtained from the ODE-based numerical kinetics simulations, whereas the solid lines were obtained with Eq. 18. Details of the ODE-based simulations are given in the Supplemental Information.
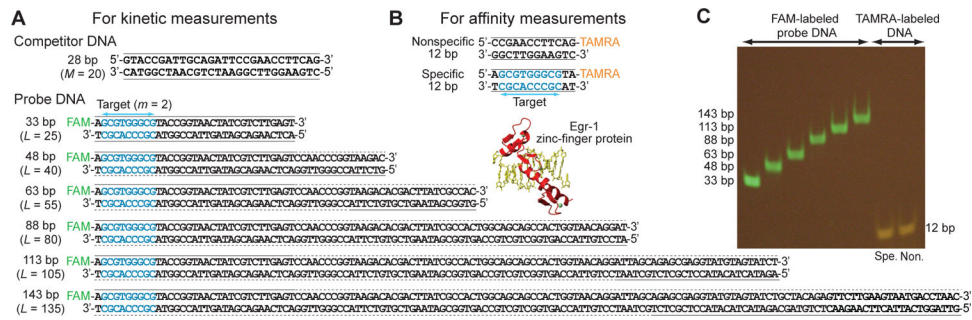
Figure 4.
DNA duplexes used in the current study on the Egr-1 zinc-finger protein. (**A**) DNA duplexes used for kinetic measurements. The solid lines indicate chemically synthesized nucleotides, whereas the dotted lines indicate enzymatically extended nucleotides. (**B**) DNA duplexes used for affinity measurements. (**C**) PAGE of the fluorescent DNA duplexes, which were visualized via fluorescence from the covalently attached FAM or TAMRA.
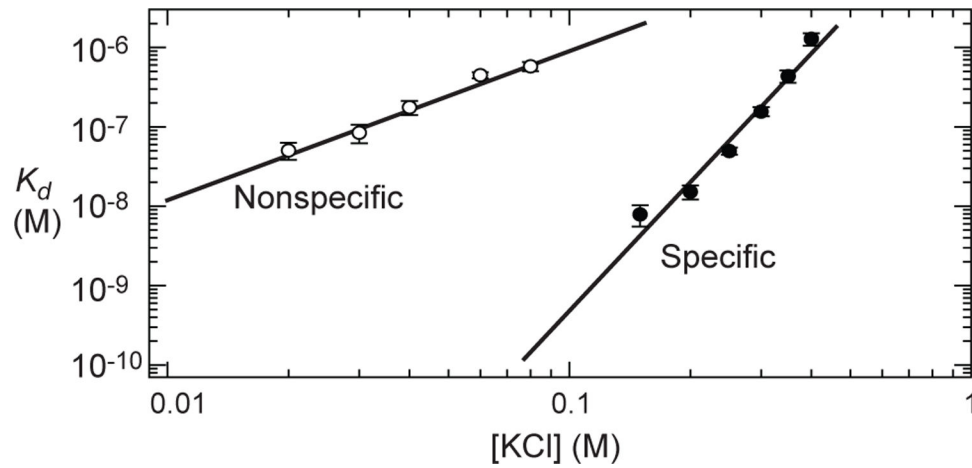
Figure 5.
Dissociation constant K_d for nonspecific and specific complexes between the Egr-1 protein and 12-bp DNA at various concentrations of KCl. These data were obtained by measuring the TAMRA fluorescence anisotropy as a function of protein concentration. For each complex, the solid line represents a linear extrapolation assuming a linear relationship (solid lines) between $\log K_d$ and $\log[\text{KCl}]$, which is based on the counterion condensation theory. [52,53]
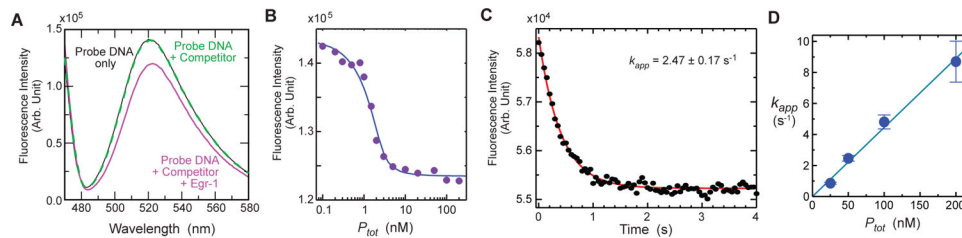
Figure 6.

FAM fluorescence data for the target association of the Egr-1 zinc-finger protein with the 113-bp probe DNA (D_{tot} = 2.5 nM) in the presence of 28-bp competitor DNA (C_{tot} = 2 μM). The buffer conditions were 10 mM Tris•HCl (pH 7.5), 80 mM KCl, and 200 nM ZnCl$_2$. (**A**) Change in the FAM emission spectra upon protein binding. The black solid line is the spectrum recorded for the probe DNA only; the green dotted line, for the probe DNA plus competitor DNA; and the magenta solid line, with the probe DNA, competitor DNA, and protein (P_{tot} = 100 nM). (**B**) FAM fluorescence intensity measured as a function of P_{tot} in the presence of the competitor DNA. (**C**) Stopped-flow time-course data of the FAM fluorescence intensity immediately after mixing the protein solution (P_{tot} = 50 nM) with the solution containing the probe and competitor DNA duplexes. The red curve represents the best fit to a mono-exponential function. (**D**) Protein-concentration dependence of the apparent pseudo-first-order kinetic rate constant k_{app} for target association. The apparent second-order rate constant for association was determined to be 4.5×10^7 M^{-1} s^{-1}. The error bars represent the standard deviations for 8 – 10 replicates.
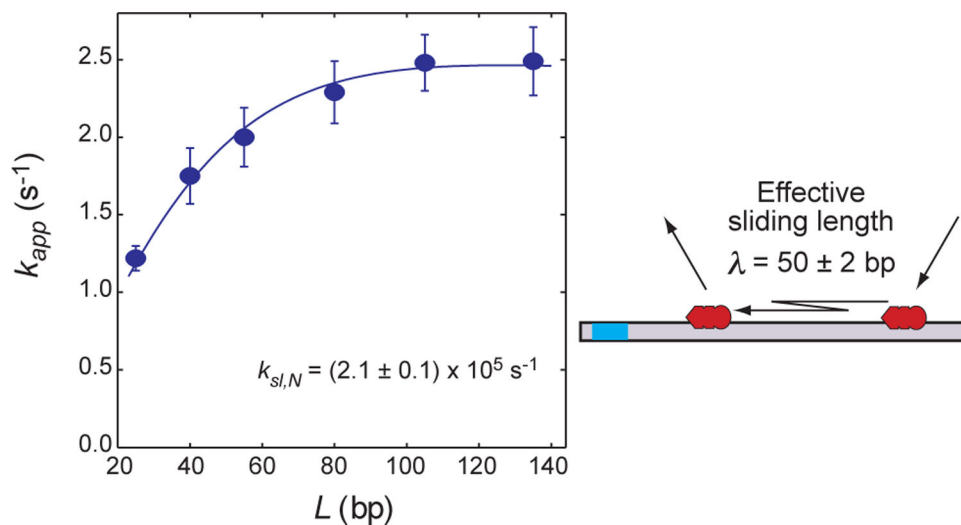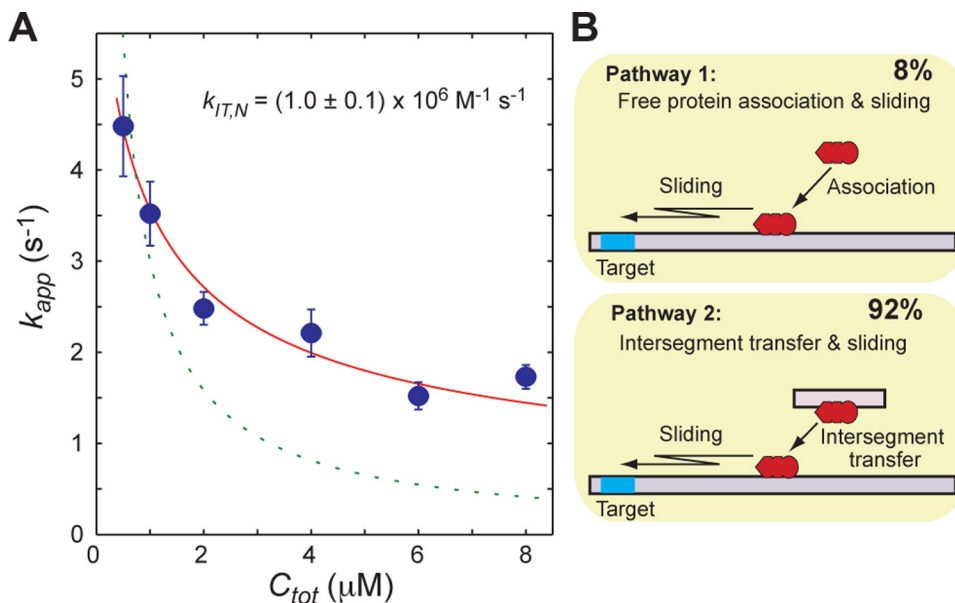
Figure 7.
DNA-length dependence of the target association kinetics measured for the Egr-1 zinc-finger protein at 80 mM KCl (D_{tot} = 2.5 nM; P_{tot} = 50 nM; and C_{tot} = 2 μM). The pseudo-first-order rate constant k_{app} for target association is plotted as a function of the total number of sites on the probe DNA. The blue curve represents the best fit to Eq. 12. The effective sliding length λ is given by Eq. 21. Note that an increase in L beyond 2λ does not enhance the target association. The error bars represent the standard deviations for 8 – 10 replicates.

Figure 8.

(**A**) Competitor DNA concentration (C_{tot}) dependence of the apparent rate constant k_{app} measured for Egr-1 (P_{tot} = 50 nM) at 80 mM KCl. The 113-bp probe DNA was used (D_{tot} = 2.5 nM). The circles represent the experimentally measured k_{app} constants. The error bars represent the standard deviations for 8 – 10 replicates. The solid red lines are the best-fit curve to Eq. 18, which accounts for intersegment transfer. The dotted green lines are the best-fit curve to Eq. 12, which does not account for intersegment transfer. (**B**) Contributions of major target association pathways under the current experimental conditions.

Table I.

Kinetic parameters for translocation of the Egr-1 zinc-finger protein on nonspecific DNA sites determined from the stopped-flow fluorescence data.

Parameters	Values and uncertainties [a]
- Sliding -	
$k_{sl,N}\,(\text{s}^{-1})$ [b]	$(2.1 \pm 0.1) \times 10^5$
$D_1\,(\mu\text{m}^2\,\text{s}^{-1})$ [c]	$(2.4 \pm 0.1) \times 10^{-2}$
- Intersegment transfer -	
$k_{it,N}\,(\text{M}^{-1}\,\text{s}^{-1})$ [d]	$(1.0 \pm 0.1) \times 10^6$
- Dissociation -	
$k_{off,N}\,(\text{s}^{-1})$ [f]	10 ± 4
$k_{out}\,(\text{s}^{-1})$ [g]	83 ± 3
- Association -	
$k_{on,N}\,(\text{M}^{-1}\,\text{s}^{-1})$ [h]	$(2.3 \pm 0.8) \times 10^6$
- Effective sliding length -	
$\lambda\,(\text{bp})$ [i]	50 ± 2

[a] Uncertainties in reported values were estimated with a 68% confidence interval in fitting.

[b] From the data shown in Figure 7.

[c] From $k_{sl,N}$ along with Eq. 15.

[d] From the data shown in Figure 8.

[f] From the data shown in Figure 8.

[g] From the data shown in Figure 7. This actually corresponds to $k_{out,CP}$ because of the strong presence of intersegment transfer.

[h] From $k_{off,N}$ and $K_{d,N}$.

[i] From $k_{sl,N}$ and k_{out} along with Eq. 21.